Received: 31 August 2021 | Revised: 5 September 2022 | Accepted: 7 October 2022

DOI: 10.1002/jnm.3073

SPECIAL ISSUE PAPER

WILEY

Comparison of 2.5D finite element formulations with perfectly matched layers for solving open axisymmetric electromagnetic cavity problems

Erik Schnaubelt | **Herbert De Gersem** | **Nicolas Marsic**

Institute for Accelerator Science and Electromagnetic Fields, Technische Universität Darmstadt, Darmstadt, Germany

Correspondence
Erik Schnaubelt, Institute for Accelerator Science and Electromagnetic Fields, Technische Universität Darmstadt, Schloßgartenstr. 8, 64289 Darmstadt, Germany.
Email: erik.schnaubelt@cern.ch

Abstract

Axial symmetry in time-harmonic electromagnetic wave problems can be exploited by considering a Fourier expansion along the angular direction, reducing fully three-dimensional computations to two-dimensional ones on an azimuthal cross section. While this transition leads to a significant decrease in computational effort, it introduces additional difficulties, which necessitate appropriate finite element (FE) formulations. By combining the latter with perfectly matched layers (PML), open problems can be considered. In this work, we compare and discuss the performance of different combinations of axisymmetric FE formulations and PMLs, using a dielectric sphere in open space as a test case. As an application example, a superconducting Fabry–Pérot photon trap is considered.

KEYWORDS

2.5D, axisymmetry, electromagnetism, finite element method, perfectly matched layers, quasi-3D, wave problems

1 | INTRODUCTION

In order to exploit the axial symmetry of a wave problem, the electromagnetic fields can be expanded into a Fourier series along the angular direction, reducing the computations to a two-dimensional (2D) azimuthal cross section, while still calculating a fully three-dimensional (3D) solution.[1] For this reason, these methods are known as *quasi-3D* or *2.5D methods*. Let us consider the Maxwell eigenvalue problem for an axisymmetric cavity V with homogeneous Dirichlet boundary conditions in a cylindrical coordinate system (r, φ, z)[1]:

$$\begin{cases} \text{Find the eigenpairs } (\mathbf{e}, \omega^2) \text{ with } \mathbf{e} \in H_0(\mathbf{curl}, V) \text{ such that} \\ \displaystyle\int_0^{2\pi}\int_\Omega \mu_\mathrm{r}^{-1}\mathbf{curl}_\mathrm{cyl}\mathbf{e}\cdot\mathbf{curl}_\mathrm{cyl}\mathbf{e}'\,\mathrm{d}\Omega\mathrm{d}\varphi - \frac{\omega^2}{c_0^2}\int_0^{2\pi}\int_\Omega \varepsilon_\mathrm{r}\mathbf{e}\cdot\mathbf{e}'\,\mathrm{d}\Omega\mathrm{d}\varphi = 0 \quad \forall\mathbf{e}' \in H_0(\mathbf{curl}, V), \end{cases} \tag{1}$$

with $\mathbf{e}(r, \varphi, z)$ the electric field, Ω a 2D azimuthal cross section of V (see Figure 1), $\mathrm{d}\Omega = r\mathrm{d}r\mathrm{d}z$, ω the angular frequency, c_0 the speed of light in vacuum and $\mathbf{curl}_\mathrm{cyl}$ the curl in cylindrical coordinates. The components of the second-

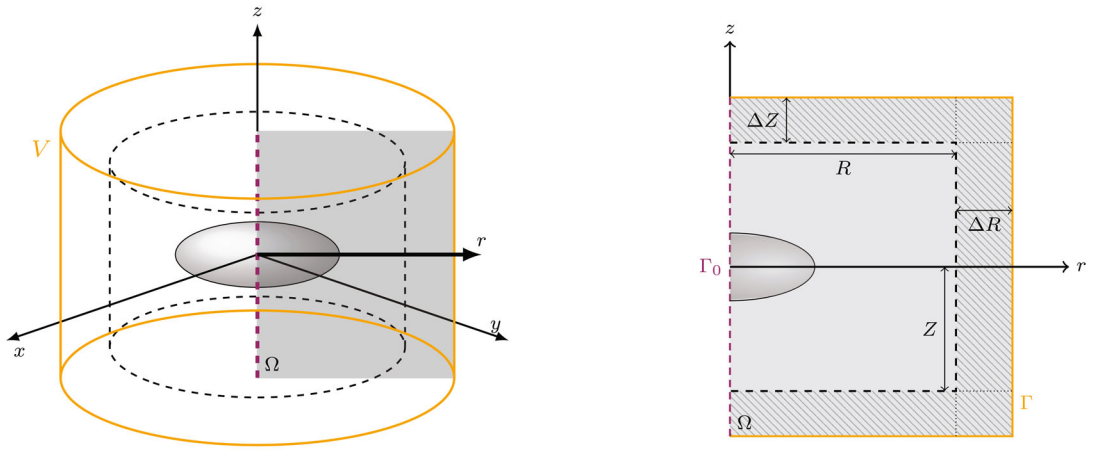

(A) Axisymmetric 3D geometry V. **(B)** 2D azimuthal cross section Ω, the PML is shown as a dashed pattern.

FIGURE 1 Model setup for axisymmetric problems and used notation; the PML can be seen between the dashed and yellow boundary

order material tensors of the relative magnetic permeability $\mu_{\mathrm{r}}^{-1} = \mathrm{diag}\left[\mu_{\mathrm{r},r}^{-1}(r,z), \mu_{\mathrm{r},\varphi}^{-1}(r,z), \mu_{\mathrm{r},z}^{-1}(r,z)\right]$ and the relative electric permittivity $\varepsilon_{\mathrm{r}} = \mathrm{diag}\left[\varepsilon_{\mathrm{r},r}(r,z), \varepsilon_{\mathrm{r},\varphi}(r,z), \varepsilon_{\mathrm{r},z}(r,z)\right]$ are assumed to be functions of the radial and axial coordinates *only* and are chosen as diagonal tensors to account for the perfectly matched layers (PMLs) as discussed in Section 3.

To take the axial symmetry into account, the electric field is expanded into a Fourier series along φ, that is,

$$\mathbf{e}(r,\varphi,z) = \begin{bmatrix} e_r^0(r,z) \\ e_\varphi^0(r,z) \\ e_z^0(r,z) \end{bmatrix} + \sum_{m=1}^{\infty} \left(\begin{bmatrix} e_r^m(r,z)\cos(m\varphi) \\ e_\varphi^m(r,z)\sin(m\varphi) \\ e_z^m(r,z)\cos(m\varphi) \end{bmatrix} + \begin{bmatrix} e_r^{-m}(r,z)\sin(m\varphi) \\ e_\varphi^{-m}(r,z)\cos(m\varphi) \\ e_z^{-m}(r,z)\sin(m\varphi) \end{bmatrix} \right), \tag{2}$$

where the Fourier coefficients $\mathbf{e}^n(r,z) = \left[e_r^n, e_\varphi^n, e_z^n\right]^T$ for $n \in \mathbb{Z}$ are independent of the angle φ. By inserting Equation (2) into formulation (1) and exploiting the orthogonality of the trigonometric functions, we rewrite the eigenvalue problem (1) for the nth eigenmode with homogeneous Dirichlet boundary conditions on the boundary Γ[1]:

$$\begin{cases} \text{For a given mode } n \in \mathbb{Z}, \text{ find the eigenpairs } (\mathbf{e}^n, \omega^2) \text{ with } \mathbf{e}^n \in \mathcal{S}^n(\Omega) \text{ such that} \\ \displaystyle\int_\Omega \mu_{\mathrm{r}}^{-1} \mathbf{curl}_n \mathbf{e}^n \cdot \mathbf{curl}_n \mathbf{e}^{n'} \,\mathrm{d}\Omega - \frac{\omega^2}{c_0^2} \int_\Omega \varepsilon_{\mathrm{r}} \mathbf{e}^n \cdot \mathbf{e}^{n'} \,\mathrm{d}\Omega = 0 \quad \forall \mathbf{e}^{n'} \in \mathcal{S}^n(\Omega), \end{cases} \tag{3}$$

where $\mathcal{S}^n(\Omega)$ is the function space of the nth Fourier coefficient and

$$\mathbf{curl}_n \mathbf{e}^n = \begin{bmatrix} -r^{-1}\left(n e_z^n + \partial_z\left(r e_\varphi^n\right)\right) \\ \partial_z e_r^n - \partial_r e_z^n \\ +r^{-1}\left(n e_r^n + \partial_r\left(r e_\varphi^n\right)\right) \end{bmatrix}.$$

2 | WELL-POSED 2.5D FORMULATION

Two approaches have been proposed in the literature for the treatment of the singularity of $\mathbf{curl}_n$ at $r = 0$ and to construct a suitable subspace of $\mathcal{S}^n(\Omega)$.[1,2] A comparison of all following strategies has been published by Schnaubelt et al[3] for closed cavity problems.

2.1 | Non-classical conditions at the symmetry axis

The first strategy consists in taking the following ansatz: $\mathbf{e}^n_{rz} = \left[e^n_r, e^n_z\right]^T \in H(\mathbf{curl}, \Omega)$ and $e^{\star,n}_\varphi = re^n_\varphi \in H^1(\Omega)$[4] and to impose *non-classical discrete conditions at the symmetry axis*.[2, Section 4.4] This approach leads to well-posed integrals while the integrands, however, remain singular. This necessitates either (i) a large number of quadrature points when using a classical Gaussian quadrature or (ii) specialized quadrature rules.[2, Section 5.1] Since the latter differ from element to element, the use of fast assembly techniques[5] is prevented. Therefore, the former approach is followed throughout this paper. In the remainder of this work, this strategy will be referred to as ansatz "A1."

2.2 | Direct construction of a subspace of $\mathcal{S}^n(\Omega)$

The second strategy is to *directly construct an appropriate subspace of* $\mathcal{S}^n(\Omega)$ in a way that guarantees the well-posedness of the variational formulation,[1,6,7] avoiding thus the need for non-classical conditions on the symmetry axis. In this approach, the problem is solved for auxiliary unknowns $u^n \in H^1(\Omega)$ and $\mathbf{U}^n \in H(\mathbf{curl}, \Omega)$ instead of the original unknowns e^n_φ and $\mathbf{e}^n_{rz}$, following the two ansätze summarized in Table 1. In what follows, we have $\mathbf{grad}_{rz} e^n_\varphi = \left[\partial_r e^n_\varphi, \partial_z e^n_\varphi\right]^T$, the unit vector along the r-axis denoted as $\widehat{\mathbf{r}}$ and the parameters $\alpha, \beta \in \mathbb{R}$.

The parameters α and β of A3(α, β) cannot be chosen freely but must satisfy certain constraints.[6,3] Following Schnaubelt et al,[3] we choose $\beta = 2$ for $n = 0$ and $\alpha = \beta = 1$ for $n \neq 0$ in this work. With this choice, ansatz A3(α, β) leads to *polynomial* integrands which is also the case for A2 when $n \neq 0$. Additionally, for some modes n, the ansätze need an additional *homogeneous Dirichlet condition* at $r = 0$ as shown in Table 2.

3 | CYLINDRICAL PERFECTLY MATCHED LAYERS AS ABSORBING BOUNDARY CONDITION

In order to model open problems, the computational domain is truncated by *cylindrical perfectly matched layers*[8] as shown in Figure 1. Let us mention that, alternatively, the domain can be truncated with an absorbing boundary condition,[9] which is however out of the scope of this paper. By mapping the spatial coordinates to complex variables, a PML introduces a complex change of the metric of the space.[10] It is worth noticing that, as the above described ansätze *do not change the metric*, all developments on cylindrical PML for general 3D problems remain valid for the 2.5D setting. A convenient way to interpret and implement the stretching of the spatial coordinates is to *incorporate it into the material tensors*[11] such that

$$\mu_r(r,z) = \widetilde{\mu}_r(r,z)\Lambda(r,z) \quad \text{and} \quad \varepsilon_r(r,z) = \widetilde{\varepsilon}_r(r,z)\Lambda(r,z), \tag{4}$$

TABLE 1 Different ansätze for constructing a subspace of $\mathcal{S}^n(\Omega)$

Mode	Ansatz A2[7]	Ansatz A3(α,β)[6, Section 1.3]
$n = 0$	$u^0 = e^0_\varphi \quad \mathbf{U}^0 = \mathbf{e}^0_{rz}$	$r^\beta u^0 = re^0_\varphi \quad \mathbf{U}^0 = \mathbf{e}^0_{rz}$
$n = \pm 1$	$u^{\pm1} = e^{\pm1}_\varphi \quad \mathbf{U}^{\pm1} = \frac{n}{r}\mathbf{e}^{\pm1}_{rz} + \frac{e^{\pm1}_\varphi}{r}\widehat{\mathbf{r}}$	$r^\beta u^{\pm1} = re^{\pm1}_\varphi \quad r^\alpha \mathbf{U}^{\pm1} = \pm\mathbf{e}^{\pm1}_{rz} + \mathbf{grad}_{rz}\left(re^{\pm1}_\varphi\right)$
$\lvert n\rvert > 1$	$u^n = e^n_\varphi \quad \mathbf{U}^n = \frac{n}{r}\mathbf{e}^n_{rz} + \frac{e^n_\varphi}{r}\widehat{\mathbf{r}}$	$r^\beta u^n = re^n_\varphi \quad r^\alpha \mathbf{U}^n = n\mathbf{e}^n_{rz} + \mathbf{grad}_{rz}\left(re^n_\varphi\right)$

TABLE 2 Conditions on the symmetry axis for the different ansätze

Mode	Ansatz A2 [19]	Ansatz A3(α,β)[6, Section 1.5]
$n = 0$	$u^0 = 0$	None
$n = \pm 1$	None	None
$\lvert n\rvert > 1$	$u^n = 0$	$u^n = 0$

with the scalar relative magnetic permeability $\widetilde{\mu}_{\mathrm{r}}(r,z)$ and electric permittivity $\widetilde{\varepsilon}_{\mathrm{r}}(r,z)$ of the medium and the modification tensor[11]

$$\Lambda(r,z)=\operatorname{diag}\left[\frac{\widetilde{r}(r)}{r}\frac{s_z(z)}{s_r(r)},\frac{r}{\widetilde{r}(r)}s_z(z)s_r(r),\frac{\widetilde{r}(r)}{r}\frac{s_r(r)}{s_z(z)}\right]. \tag{5}$$

Herein, we have used the complex-valued stretching functions

$$s_r(r)=\begin{cases}1-ip_r(r) & \text{if } r>R,\\ 1 & \text{else,}\end{cases}\quad\text{and}\quad s_z(z)=\begin{cases}1-ip_z(z) & \text{if } |z|>Z,\\ 1 & \text{else,}\end{cases}\quad\text{and}\quad \widetilde{r}(r)=R+\int_R^r s_r(r')\mathrm{d}r', \tag{6}$$

where R (resp. Z) is the distance between the $r-$axis (resp. $z-$axis) and the PML in the $r-$direction (resp. z-direction) as shown in Figure 1. The different types of PMLs are then distinguished by their damping functions p_r and p_z. In this work, six different damping functions will be compared as summarized in Table 3. Here, ΔR (resp. ΔZ) is the thickness of the PML in r-direction (resp. z-direction) as illustrated in Figure 1, a (in rad/m) is the absorption parameter[2] and $\widetilde{k}=\mathrm{Re}\,(\omega)/c_0$ is the real part of the wavenumber. Due to the dependency of $\widetilde{k}$ on the angular frequency, all damping functions of Table 3 except for the constant one lead to *nonlinear eigenvalue problems*[12] when inserted into formulation (3).

Finally, since the electric field is assumed to have decayed to zero on the boundary Γ, homogeneous Dirichlet boundary conditions $\mathbf{n}\times\mathbf{e}^n\times\mathbf{n}=0$ are imposed on Γ with the outward pointing unit vector $\mathbf{n}$, recovering the formulation (3).

4 | NUMERICAL EXPERIMENTS ON A DIELECTRIC SPHERE IN VOID

In order to validate and compare the method, a systematic analysis has been performed on a dielectric resonating sphere surrounded by air with radius $r=1\mathrm{m}$ and with a relative electric permittivity $\varepsilon_{\mathrm{r}}=40$, for which closed-form solutions of the eigenvalue problem (3) are well-known.[16] Since the eigenfrequencies ω are known, the pre-computed value for $\widetilde{k}$ is used for the damping functions, *converting thus the nonlinear eigenvalue problem into a classical* generalized one.

This section is structured as follows: in Section 4.1, the approaches are validated by checking the convergence with respect to the mesh refinement. Afterwards, the accuracy of the approaches is compared with respect to the influence of the PML thickness and distance in Section 4.2 and with respect to the damping parameter a in Section 4.3. Last, in Section 4.4, a comparison of the computational cost of the approaches can be found. *For the sake of compactness, only a selection of the numerical experiments carried out for the systematic analysis is shown. However, the data shown are representative for all numerical experiments carried out.*

To carry out the analysis, the approaches have been implemented in a homemade high-order open-source finite element (FE) code.*

TABLE 3 Damping functions considered in this work[8,13,14,15]

Function	Abbreviation	$p_r(r)$	$p_z(z)$
Constant	c.	1	1
Constant parameterized	c.p.	$\frac{a}{k}$	$\frac{a}{k}$
Linear	l.	$\frac{a}{k}\frac{r-R}{\Delta R}$	$\frac{a}{k}\frac{\lvert z-\mathrm{sgn}(z)Z\rvert}{\Delta Z}$
Quadratic	q.	$\frac{a}{k}\left(\frac{r-R}{\Delta R}\right)^2$	$\frac{a}{k}\left(\frac{z-\mathrm{sgn}(z)Z}{\Delta Z}\right)^2$
Hyperbolic	h.	$\frac{a}{k}\frac{1}{\Delta R-(r-R)}$	$\frac{a}{k}\frac{1}{\Delta Z-\lvert z-\mathrm{sgn}(z)Z\rvert}$
Shifted hyperbolic	h.s.	$\frac{a}{k}\frac{1}{\Delta R-(r-R)}+\frac{a}{k}\frac{1}{\Delta R}$	$\frac{a}{k}\frac{1}{\Delta Z-\lvert z-\mathrm{sgn}(z)Z\rvert}+\frac{a}{k}\frac{1}{\Delta Z}$

4.1 | Validation: Convergence with respect to the mesh refinement

First, the approaches are validated by investigating the convergence of the numerically computed eigenfrequencies with respect to the mesh refinement. To this end, a structured fourth order triangular mesh as shown in Figure 2 is refined by successively uniformly splitting each triangle into four subtriangles. Figure 4 shows the decrease of the relative error between the numerically computed eigenfrequency and its analytical counterpart for different mesh refinement levels, $n \in \{1, 2\}$ and for all 2.5D ansätze as described above. In order to simplify the discussion, the PML distance and thickness are chosen equal† and are fixed to $R = Z = \Delta R = \Delta Z = 1\lambda$ with the wavelength λ. Furthermore, we choose $a = 5\text{rad/m}$. These choices have been made to ensure converging solutions (compare the following sections for a justification). A second order FE method is used, thus a convergence slope of 4 for the eigenfrequency with respect to the mesh refinement is expected.[17]

All combinations of 2.5D ansätze and PML damping functions *lead to converging solutions* close to or exceeding the expected convergence slope. Let us note that this is not an isolated case but has been observed for all n and all investigated modes. The numerically computed solutions for the ansätze A2 and A3 coincide, as it has also been the case for the closed cavity problems.[3] Since this holds true for all following test cases, in particular for all n, different FE orders and PML damping functions, *only one of the two ansätze is shown for the remainder of this work*.

While A2 and A3 outperformed A1 for closed cavity problems leading to smaller relative errors for the same mesh,[3] a similar conclusion cannot be drawn for the case of open cavities. For the latter, the absolute value of the relative error for the different 2.5D ansätze depends on the investigated eigenmode, n and the chosen PML parameters. Last, little differences are observed when comparing the different damping profiles. As shown in the next subsection, this is due to the particular choice of a, R, Z, ΔR and ΔZ.

However, before analyzing the influence of the PML parameters, the influence of the FE order on the convergence slope will be checked. The decrease of the relative error can be seen in Figure 3 for different FE orders p. As it has been

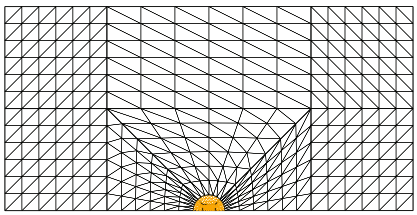

FIGURE 2 Illustration of a structured triangular mesh used for the mesh refinement convergence tests, the dielectric sphere is shown in orange

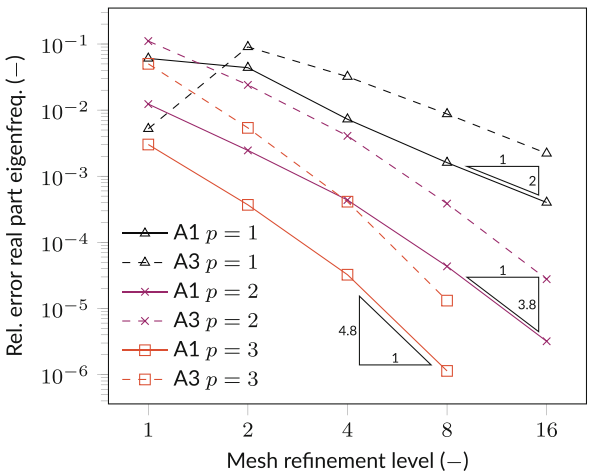

(A) Relative error of the real part of the eigenfrequency.

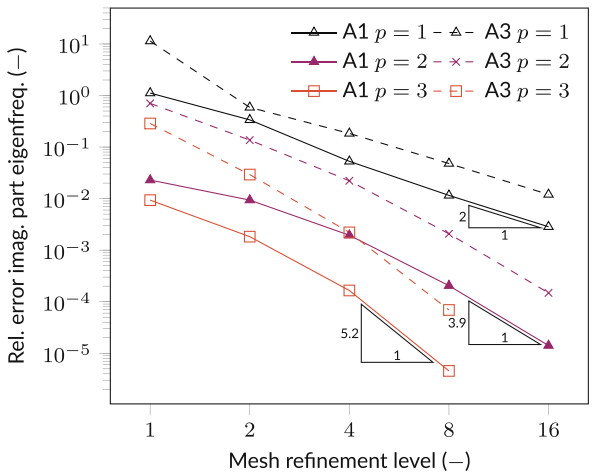

(B) Relative error of the imaginary part of the eigenfrequency.

FIGURE 3 Convergence results for the fundamental mode TE_{1m1}, different FE orders p, $R = Z = \Delta R = \Delta Z = 1\lambda$ and $n = 1$. The index m reflects the degeneracy of the modes[16] and a constant damping function is used

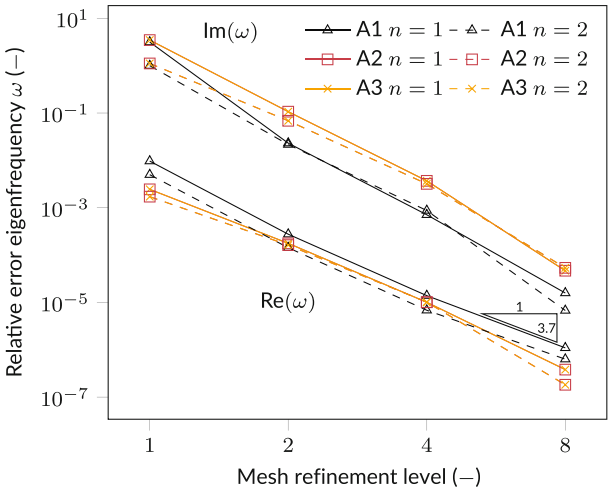

(A) Constant damping function.

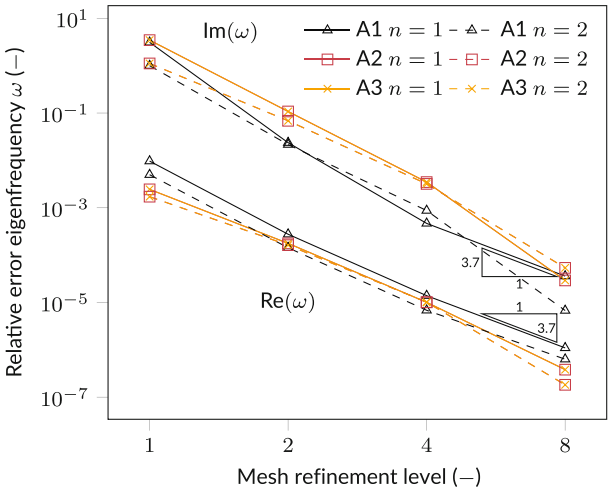

(B) Constant parameterized damping function.

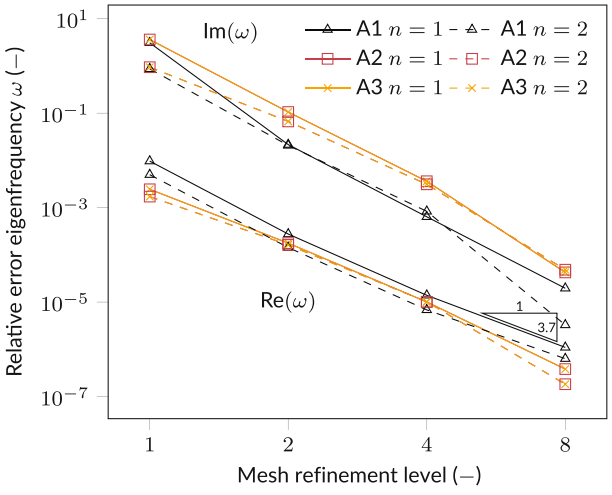

(C) Linear damping function.

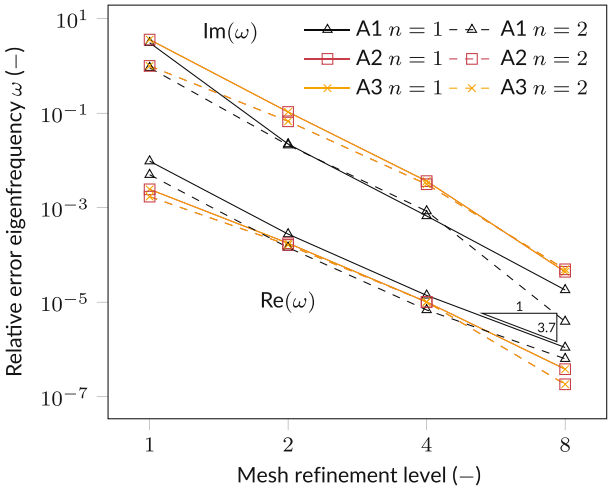

(D) Quadratic damping function.

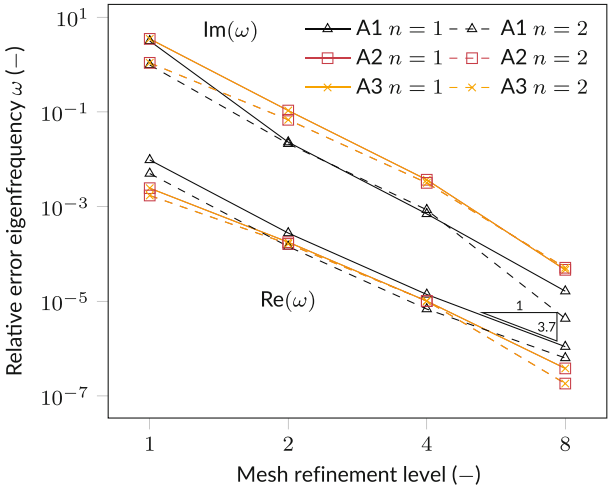

(E) Hyperbolic damping function.

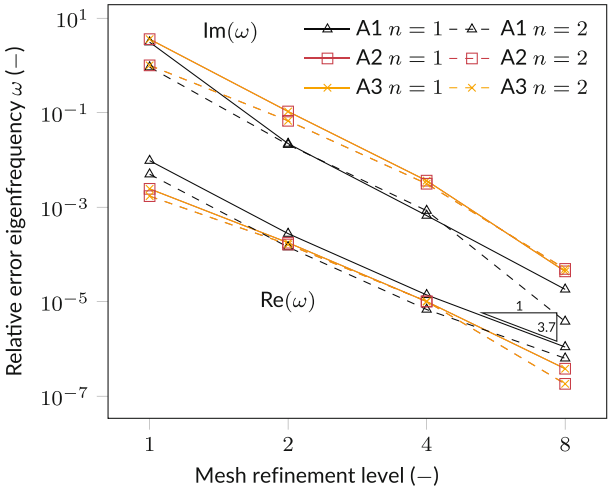

(F) Shifted hyperbolic damping function.

FIGURE 4 Convergence results for the TM_{4m1} mode with $R = Z = \Delta R = \Delta Z = 1\lambda$, $n \in \{1, 2\}$, $a = 5\,\mathrm{rad/m}$ and a second order FE method. The lowest slope is marked by a triangle, the upper (lower) curves represent the imaginary (real) part

established that the difference between the different damping functions is negligible for this choice of R, Z, ΔR, ΔZ and a, only the constant one is shown here for the sake of conciseness. As the FE order is increased, the expected convergence slope is matched for first and second order, but this is not the case for the third order method where a slope of 6 is expected. A possible explanation for this behavior is the geometrical error which is introduced when approximating the circular boundary of the sphere by polynomials. This problem could be alleviated by the use of isogeometric methods.[18]

4.2 | Accuracy comparison: Convergence with respect to the PML thickness and distance

In this section, the influence of the PML thickness and distance is investigated. Figure 5 shows the relative error of the eigenfrequency as a function of the PML thickness and distance $R = Z = \Delta R = \Delta Z = s_{\mathrm{PML}}$ in terms of the wavelength λ for all damping functions. To this end, an unstructured mesh is used in order to keep the same mesh density inside the PML when considering different s_{PML}. In the figure, the results for ansatz A1, $n = 2$ and a third-order method are depicted for the sake of conciseness. However, the same conclusions can be drawn for the other ansätze and FE orders as well as for other n and eigenmodes.

For increasing PML thickness and distance, the differences between the damping functions become increasingly negligible, with the damping function c.p. being the only exception (compare especially the results for the imaginary part). This is approximately already the case for $s_{\mathrm{PML}} \geq \lambda$ and hence, this value has been chosen for the previous and the subsequent test cases. Let us note that, while the number of degrees of freedom obviously increases with s_{PML}, the computational cost does not become prohibitive with 2.5D methods, in contrast to full 3D computations, due to the 2D mesh used.

4.3 | Accuracy comparison: Convergence with respect to the absorption parameter

As a last numerical experiment on the dielectric sphere, the influence of the absorption parameter a on the accuracy of the solution is investigated in this section. To this end, the evolution of the relative error of the eigenfrequency w.r.t. a is shown in Figure 6 for ansatz A3 and $R = Z = \Delta R = \Delta Z = 1\lambda$. Furthermore, since the influence of a also depends on the number of mesh elements per wavelength inside the PML $n^{\lambda}_{\mathrm{PML}}$, the latter is swept between 2 and 32 while the mesh size inside the non-PML part of the computational domain is kept constant at eight elements per λ. To achieve this, an unstructured triangular mesh is used.

For $n^{\lambda}_{\mathrm{PML}} = 2$, the accuracy of the solution varies with a over the whole interval of investigated absorption parameters. However, as $n^{\lambda}_{\mathrm{PML}}$ increases to $n^{\lambda}_{\mathrm{PML}} = 32$, there exists a threshold a_{t} after which the solution is approximately

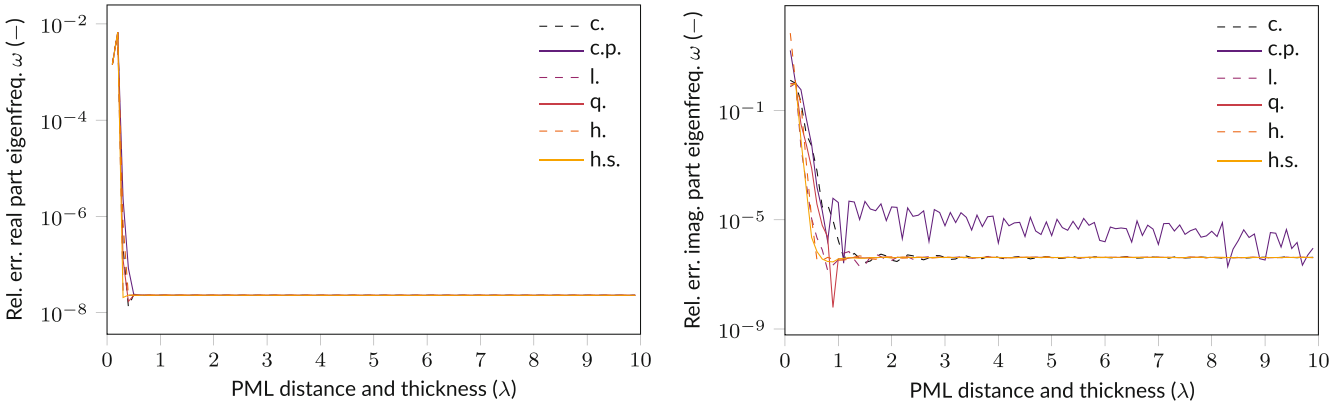

(A) Relative error of the real part of the eigenfrequency.

(B) Relative error of the imaginary part of the eigenfrequency.

FIGURE 5 Influence of the perfectly matched layer thickness and distance on the relative error of the numerically computed eigenfrequency of the TE_{4m1} mode of the free dielectric sphere. A third order FE method, $n = 2$, $a = 5\mathrm{rad/m}$ and ansatz A1 are used

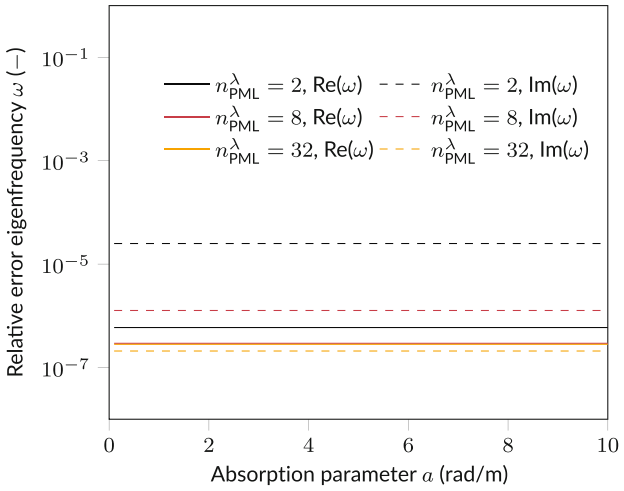

(A) Constant damping function.

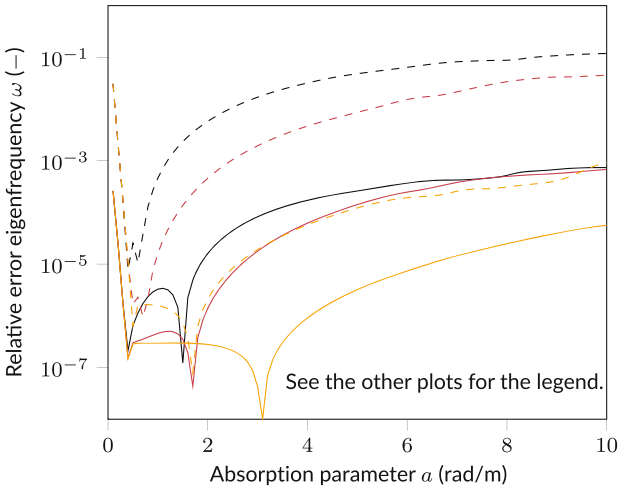

(B) Constant parameterized damping function.

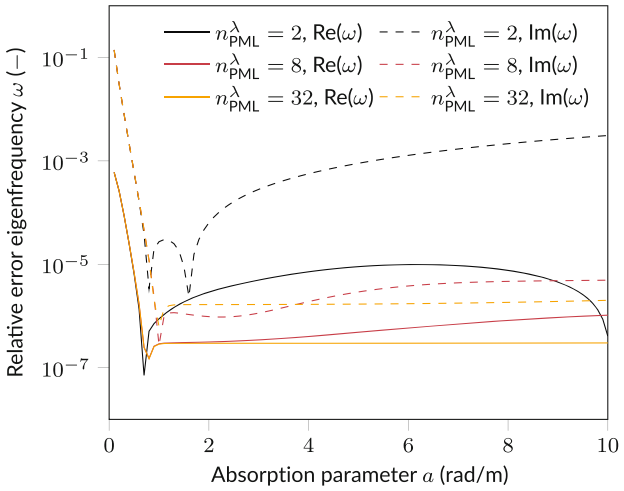

(C) Linear damping function.

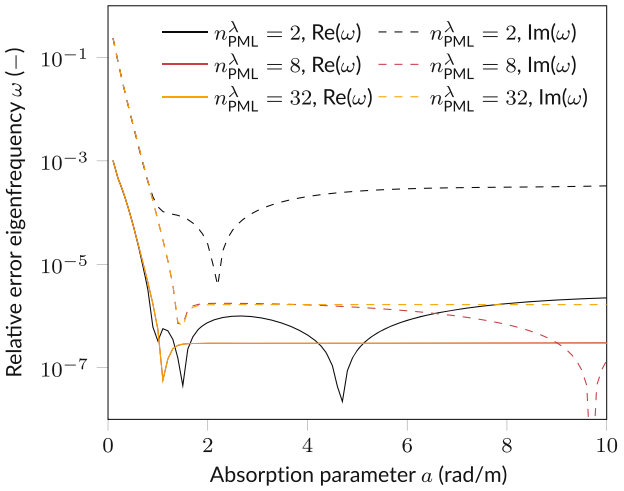

(D) Quadratic damping function.

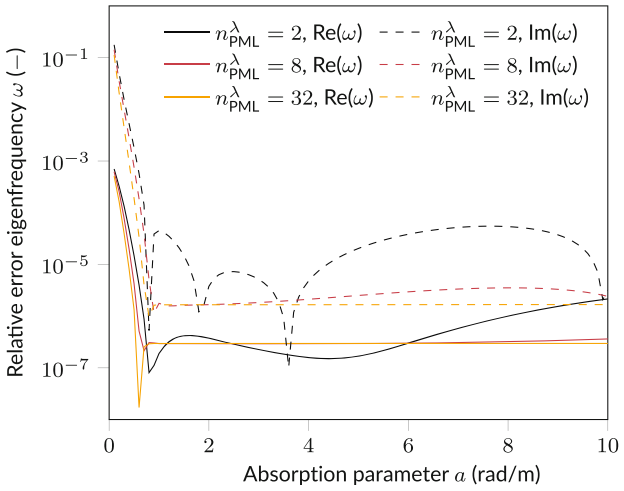

(E) Hyperbolic damping function.

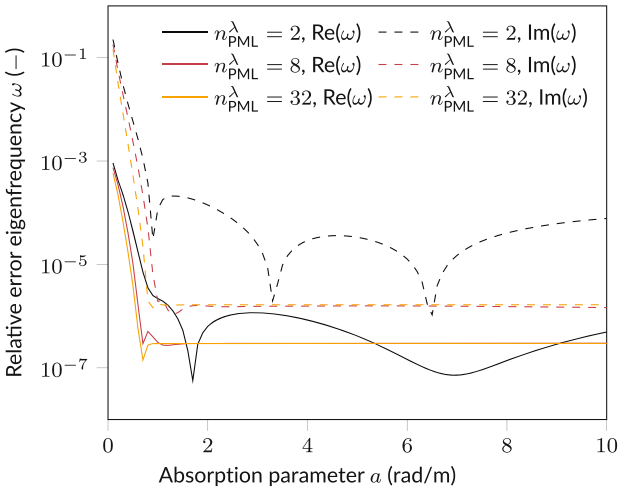

(F) Shifted hyperbolic damping function.

FIGURE 6 Influence of the absorption parameter on the numerically computed eigenfrequency of the TE_{4m1} mode. A third order FE method, $n = 2$, $R = Z = \Delta R = \Delta Z = 1\lambda$ and ansatz A2 are used

constant w.r.t. a. Again, the constant parameterized damping function forms an exception since its behavior is sensitive to a, even for fine meshes inside the PML. In particular, no a_t can be found for the latter damping profile. For all other damping functions, assuming a sufficient spatial resolution in the PML region, the influence of a is negligible for $a > a_t$. However, the threshold depends, among others, on the investigated eigenmode and on n. Due to this behavior, $a = 5\text{rad/s} > a_t$ has been chosen for the previous test cases.

Furthermore, assuming that the threshold is exceeded, the damping functions yield comparable solutions, even in the constant PML case, which does not involve the parameter a. Last, the other 2.5D ansätze lead to the same conclusions as well as different n, FE orders and investigated eigenmodes. As already stated, the latter will, however, influence the value of a_t.

4.4 | Computational cost

Before concluding this section about the dielectric sphere in void, let us address the question of the computational cost. In particular, we focus in this section on the simulations carried out in Section 4.3 and restrict the damping parameter a to the set a {1, 5, 10} rad/m for conciseness reasons.

The computational cost is usually divided in two parts: the cost of the *assembly* of the discrete matrices and the cost of *solving* the associated eigenvalue problem. Regarding the assembly cost, we provide the number of elementary FE terms associated with the different ansätze in Table 4, which clearly shows that, while A2 and A3 demand less integration points for the assembly than A1, they require more elementary FE terms than A1. In Schnaubelt et al,[3] a discussion comparing the three ansätze in terms of accuracy with respect to the number of integration points is available.‡

Let us now focus on the computational effort required for computing the eigenpairs $(\mathbf{e}, \omega^2)$ of (1). Our implementation relies on the Krylov–Schur method,[19] as provided by the SLEPc library.[20] Additionally, the eigenvalue problem is transformed with the Shift-and-Invert approach[21] and the underlying LU factorization is carried out with the MUMPS mutlifrontal direct solver.[22] In our case, this latter step is the most computationally consuming part of the eigenvalue solver and, for this reason, we concentrate only on this part in the following paragraph. But before that, let us mention that in all cases the Krylov–Schur method converged in one iteration, as the spectral shift was selected with the analytical solution.

The wall-clock times associated with the cases $n^{\lambda}_{\text{PML}} = 2$, $n^{\lambda}_{\text{PML}} = 8$ and $n^{\lambda}_{\text{PML}} = 32$ are provided in Table 5, which shows the results for the constant PML case only. Nonetheless, the timings are equivalent with the other PMLs and the considered values of a, up to 1s. Those data are the average value over 5 different runs, the associated standard deviation being smaller than 1s in every case. In all these different scenarios, the wall-clock time of the A1 ansatz is the smallest, with a relative difference of approximately 14% when compared with A2 and A3, the latter two exhibiting approximately the same wall-clock time. Explaining this phenomenon is a delicate task, but a few differences between

TABLE 4 Number of elementary FE terms associated with the different ansätze

Ansatz	Number of FE terms
A1	7
A2	30
A3	15

TABLE 5 Time required for solving the eigenvalue problem (1) for the constant perfectly matched layer (PML; values in seconds, averaged value over 5 runs, same setting as in Section 4.3, the data regarding the other PMLs—for $a \in \{1, 5, 10\}\,\text{rad/m}$—are the same, up to 1s)

n^{λ}_{PML}	Ansatz		
	A1	A2	A3
2	18	21	21
8	20	23	23
32	37	43	43

the three ansätze are worth mentioning. First, the matrices resulting from A1 are sightly smaller, because of the use of boundary conditions on the symmetry axis. Nonetheless, this difference decreases as the number of mesh elements in Ω increases. Second, the sparsity patterns associated with each ansatz are very different from each other. As a notable result, the order of the largest frontal matrix[22] (as reported by MUMPS) is systematically larger (yet only by approximately 1%) with A1 when compared with A2 and A3, the latter two exhibiting the same order. Finally, the number of off-diagonal pivots is also very different in the matrices resulting from the different ansätze. In particular, A1 (resp. A3) is systematically associated with the smallest (resp. largest) number of off-diagonal pivots. Concerning the memory usage of the MUMPS solver, it varies by less than 1% when comparing the three ansätze on the same test case.

To conclude this section, let us discuss briefly the case of nonlinear eigenvalue problems, when solved with a contour integral method.[23] In a nutshell, this approach requires the solution of many linear systems that have the same structure as the one found in the Shift-and-Invert transformation, up to the "shift" which is different for each system. Therefore, our previous analysis for the linear case applies as well. However, this computational cost must be paid more than once in the nonlinear case, one for each linear system. Nonetheless, in the case of a contour integral approach, the aforementioned linear systems can be solved in a concurrent way and independently from each other, exhibiting thus good scaling properties.

5 | SIMULATION OF AN ULTRAHIGH FINESSE FABRY–PÉROT SUPERCONDUCTING RESONATOR

As an application example, an ultrahigh finesse Fabry–Pérot superconducting resonator, whose dimensions are similar to the one built by Kuhr et al,[24] is simulated (see Figure 7). Such devices find applications in quantum computing, by creating a quantum system consisting of a *single* trapped photon.[25] In this work, we are interested in computing the resonance frequency and damping time of the 9th trapping mode[24] numerically. This is a computationally demanding task which requires the usage of clusters in 3D.[26] The cavity is not axially symmetric but elliptic. Nonetheless, its two radii of curvature are close to each other (40.6mm and 39.4mm).[24] For this reason, it will be approximated as axisymmetric to benefit from 2.5D methods. The 2.5D results will subsequently be compared to the ones achieved with a full 3D FE simulation of the elliptic cavity.[26]

The relation between the angular frequency ω computed in the eigenvalue problem and the cavity resonance frequency f and damping time τ reads

$$\omega^2 = \left(2\pi f + i\frac{1}{\tau}\right)^2. \tag{7}$$

The constant damping function will be used for this numerical study, as it was established in the previous test case as an appropriate choice and naturally leads to a classical generalized eigenvalue problem. Furthermore, after a dedicated sensitivity analysis, the PML thickness and distance are chosen as one wavelength. An unstructured second order

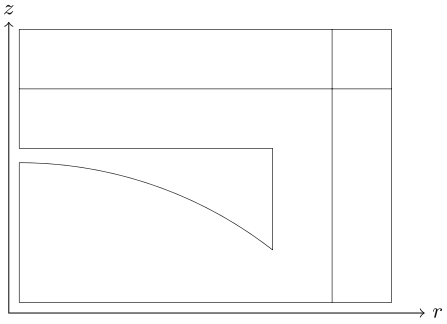

FIGURE 7 The upper half of the azimuthal cross section of the considered superconducting resonator, its radius is 25mm, the radius of the curvature is 40.6mm and the distance between the apexes is 27.57mm.[24] Due to symmetry considerations, only the upper half of the cross section needs to be simulated. The model is truncated by perfectly matched layers in axial and radial direction

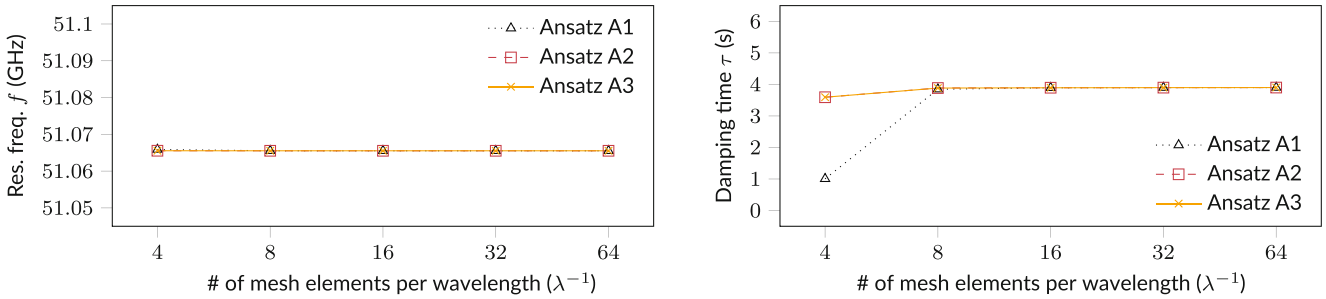

(A) Resonance frequency f (2.5D method). **(B)** Damping time τ (2.5D method).

FIGURE 8 Numerically computed resonance frequency and damping time of the trapping mode of the superconducting cavity approximated as axisymmetric. A constant damping function, $R = Z = \Delta R = \Delta Z = 1\lambda$ and a third order 2.5D FE method have been used

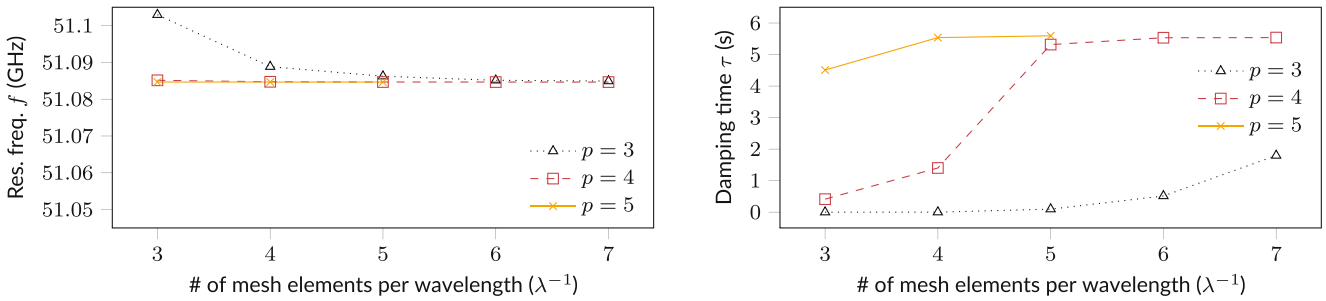

(A) Resonance frequency f (3D method). **(B)** Damping time τ (3D method).

FIGURE 9 Numerically computed[26] resonance frequency and damping time of the trapping mode of the 3D superconducting cavity. A hyperbolic damping function, $R = Z = \Delta R = \Delta Z = 1\lambda$ and a FE method of order p are used

triangular mesh is used. The evolution of the resonance frequency and damping time with the number of mesh elements can be seen in Figure 8. Convergence is reached both for f and τ for all different 2.5D ansätze. Furthermore, the numerically computed values are comparable§ to the ones achieved using a 3D simulation of the actual non-axisymmetric geometry[26] (see Figure 9). For the latter, however, the simulation used significantly less mesh elements per wavelength due to memory limitations caused by the 3D meshes. Hence, the convergence is not as clearly visible as in the 2.5D case. Furthermore, the 2.5D results have been generated on a laptop computer with 16 GB of RAM with simulation times in the range of few minutes while the 3D simulation has been run on a cluster using 120 computing nodes with 64 GB of RAM per node which still needed hours of run time. By drastically reducing run times, 2.5D methods enable the usage of optimization or uncertainty quantification methods for (almost) axisymmetric problems.

6 | CONCLUSIONS

This paper compared three different 2.5D ansätze in combination with six different damping profiles for cylindrical perfectly matched layers to treat open three-dimensional time-harmonic electromagnetic wave problems in axisymmetric geometries. Given an appropriate choice of the absorption parameter as well as PML thickness and distance, it has been shown that all combinations yield accurate results when computing the eigenfrequencies of a free dielectric sphere, with the constant parameterized damping function being an exception due to its sensitivity to the choice of a and s_{PML}. The constant damping profile has been proposed as a simple and suitable choice since first, it does not turn the generalized eigenvalue problem into a nonlinear one, as it is parameter free, in contrast to the other profiles. Second, performance differences between the different damping profiles have been observed to be negligible assuming that the PML size and distance is chosen big enough, which is not computationally prohibitive thanks to the 2D mesh used. It has been shown that ansatz A1 leads to slightly smaller computational times when solving the eigenvalue problem. Hence, we propose the combination of ansatz A1 and constant damping profile as a simple but appropriate choice. While this

proposal is not an optimal choice and could be improved upon by an independent study of the influence of the PML thickness and distance, it leads to a drastic reduction of computational effort of 2.5D methods compared to 3D methods as demonstrated on an ultrahigh finesse Fabry–Pérot superconducting resonator.

AUTHOR CONTRIBUTIONS

Nicolas Marsic, Erik Schnaubelt, Herbert De Gersem: Conceptualization, writing—review & editing. **Erik Schnaubelt:** Formal analysis, investigation, visualization, writing—original draft. **Nicolas Marsic:** Project administration. **Herbert De Gersem:** Resources. **Erik Schnaubelt, Nicolas Marsic:** Software, validation. All authors have read and commented the manuscript.

ACKNOWLEDGMENTS

The authors would like to express their gratitude to Dr. Axel Modave (Institut Polytechnique de Paris) for his valuable advice and the fruitful discussions on PMLs. The authors would also like to thank Ms. Heike Koch, Mr. Achim Wagner, Mr. Christian Schmitt, Mr. Dragos Munteanu and Dr. Wolfgang Müller (all Technische Universität Darmstadt) for the administrative and technical support. Open Access funding enabled and organized by Projekt DEAL.

CONFLICT OF INTEREST

The authors declare no conflict of interest.

DATA AVAILABILITY STATEMENT

The data that support the findings of this study are available from the corresponding author upon reasonable request.

ORCID

Erik Schnaubelt https://orcid.org/0000-0003-3224-6729
Herbert De Gersem https://orcid.org/0000-0003-2709-2518
Nicolas Marsic https://orcid.org/0000-0001-6825-0530

ENDNOTES

* See https://gitlab.onelab.info/gmsh/small_fem/-/blob/master/simulation/Quasi3DPML.cpp

† This choice is in general not optimal and the influence of the PML distance and thickness on the numerical accuracy and efficiency should be studied independently. However, for the applications studied in this paper, the choice $R = Z = \Delta R = \Delta Z$ has been found to be appropriate.

‡ Let us note that the wall-clock time associated with the assembly of A1, A2 and A3 cannot be compared with our homemade FE code. Indeed, this code exhibits two distinct assembly kernels: a "fast" one exploiting cache locality (as discussed in Marsic et al[5]) and a "slow" one that does not. In the current status of the implementation, the A2 and A3 ansätze do not fit into the "fast" kernel while the A1 does. In a high-order FE context, this leads to very large differences in the assembly time. Before concluding this footnote, let us mention that the use of the "slow" kernel is not due to a fundamental limitation of the A2 and A3 ansätze, but to technical details related to the implementation itself.

§ Thus, the 2.5D results support the validity of the original 3D simulation since they are in the same order of magnitude.

REFERENCES

1. Lacoste P. Solution of Maxwell equation in axisymmetric geometry by Fourier series decomposition and by use of H(rot) conforming finite element. *Numer Math*. 2000;84(4):577-609. doi:10.1007/s002110050011
2. Chinellato O. *The Complex-Symmetric Jacobi-Davidson Algorithm and its Application to the Computation of some Resonance Frequencies of Anisotropic Lossy Axisymmetric Cavities*. PhD thesis. Eidgenössische Technische Hochschule Zürich; 2005.
3. Schnaubelt E, Marsic N, De Gersem H. A comparison between different formulations for solving axisymmetric time-harmonic electromagnetic wave problems. In: van Beurden M, Budko N, Schilders W, eds. *Scientific Computing in Electrical Engineering. 36 of Mathematics in Industry*. Springer; 2021:169-177.
4. Lee JF, Wilkins GM, Mitra R. Finite-element analysis of axisymmetric cavity resonator using a hybrid edge element technique. *IEEE Trans Microw Theory Tech*. 1993;41(11):1981-1987. doi:10.1109/22.273425
5. Marsic N, Geuzaine C. Efficient finite element assembly of high order Whitney forms. *IET Sci Meas Technol*. 2015;9(2):204-210. doi:10.1049/iet-smt.2014.0199
6. Cambon S. *Méthode d'éléments finis d'ordre élevé et d'équations intégrales pour la résolution de problème de furtivité radar d'objets à symétrie de révolution*. PhD thesis. Institut National des Sciences Appliquées de Toulouse; 2012.

7. de Oh M. Rham complexes arising from Fourier finite element methods in axisymmetric domains. *Comput Math Appl*. 2015;70(8):2063-2073. doi:10.1016/j.camwa.2015.08.020
8. Berenger JP. A perfectly matched layer for the absorption of electromagnetic waves. *J Comput Phys*. 1994;114(2):185-200. doi:10.1006/jcph.1994.1159
9. Givoli D. Computational absorbing boundaries. In: Marburg S, Nolte B, eds. *Computational Acoustics of Noise Propagation in Fluids - Finite and Boundary Element Methods*. Springer; 2008:145-166.
10. Teixeira F, Chew W. Differential forms, metrics, and the reflectionless absorption of electromagnetic waves. *J Electromagn Waves Appl*. 1999;13(5):665-686. doi:10.1163/156939399X01104
11. Teixeira F, Chew W. Systematic derivation of anisotropic PML absorbing media in cylindrical and spherical coordinates. *IEEE Microw Guided Wave Lett*. 1997;7(11):371-373. doi:10.1109/75.641424
12. Güttel S, Tisseur F. The nonlinear eigenvalue problem. *Acta Numerica*. 2017;26:1-94. doi:10.1017/S0962492917000034
13. Modave A. *Absorbing Layers for Wave-Like Time-Dependent Problems—Design, Discretization and Optimization*. PhD thesis. Université de Liège; 2013.
14. Greenwood A, Jin JM. A novel efficient algorithm for scattering from a complex BOR using mixed finite elements and cylindrical PML. *IEEE Trans Antennas Propag*. 1999;47(4):620-629. doi:10.1109/8.768800
15. Bermúdez A, Hervella-Nieto L, Prieto A, Rodríguez R. An exact bounded PML for the Helmholtz equation. *Comptes Rendus Mathematique*. 2004;339(11):803-808. doi:10.1016/j.crma.2004.10.006
16. Gastine M, Courtois L, Dormann J. Electromagnetic resonances of free dielectric spheres. *IEEE Trans Microw Theory Tech*. 1967;15(12):694-700. doi:10.1109/TMTT.1967.1126568
17. Sauter S. *Hp*-finite elements for elliptic eigenvalue problems: error estimates which are explicit with respect to λ, h, and p. *SIAM J Numer Anal*. 2010;48(1):95-108. doi:10.1137/070702515
18. Simona A, Bonaventura L, de Falco C, Schöps S. IsoGeometric approximations for electromagnetic problems in axisymmetric domains. *Comput Methods Appl Mech Eng*. 2020;369:113211. doi:10.1016/j.cma.2020.113211
19. Stewart GW. A Krylov-Schur algorithm for large eigenproblems. *SIAM J Matrix Anal Appl*. 2002;23(3):601-614. doi:10.1137/S0895479800371529
20. Hernandez V, Roman JE, Vidal V. SLEPc: a scalable and flexible toolkit for the solution of eigenvalue problems. *ACM Trans Math Softw*. 2005;31(3):351-362. doi:10.1145/1089014.1089019
21. Saad Y. *Numerical Methods for Large Eigenvalue Problems*. Society for Industrial and Applied Mathematics; 2011.
22. Amestoy PR, Duff IS, Koster J, L'Excellent JY. A fully asynchronous multifrontal solver using distributed dynamic scheduling. *SIAM J Matrix Anal Appl*. 2001;23(1):15-41. doi:10.1137/S0895479899358194
23. Güttel S, Tisseur F. The nonlinear eigenvalue problem. *Acta Numerica*. 2017;26:1-94. doi:10.1017/S0962492917000034
24. Kuhr S, Gleyzes S, Guerlin C, et al. Ultrahigh finesse Fabry-Pérot superconducting resonator. *Appl Phys Lett*. 2007;90(16):164101. doi:10.1063/1.2724816
25. Gleyzes S, Kuhr S, Guerlin C, et al. Quantum jumps of light recording the birth and death of a photon in a cavity. *Nature*. 2007;446(7133):297-300. doi:10.1038/nature05589
26. Marsic N, De Gersem H, Demésy G, Nicolet A, Geuzaine C. Modal analysis of the ultrahigh finesse Haroche QED cavity. *New J Phys*. 2018;20(4):043058. doi:10.1088/1367-2630/aab6fd

How to cite this article: Schnaubelt E, De Gersem H, Marsic N. Comparison of 2.5D finite element formulations with perfectly matched layers for solving open axisymmetric electromagnetic cavity problems. *Int J Numer Model*. 2023;36(3):e3073. doi:10.1002/jnm.3073